Journal of Applied Physics

RESEARCH ARTICLE | FEBRUARY 11 2025

Phase-separated amorphous Si_2BN: A computational study

Special Collection: Disordered Materials at the Atomic Scale

Murat Durandurdu

J. Appl. Phys. 137, 065104 (2025)
https://doi.org/10.1063/5.0244715

Journal of Applied Physics ARTICLE pubs.aip.org/aip/jap

Phase-separated amorphous Si_2BN: A computational study

Cite as: J. Appl. Phys. **137**, 065104 (2025); doi: 10.1063/5.0244715
Submitted: 21 October 2024 · Accepted: 27 January 2025 ·
Published Online: 11 February 2025

Murat Durandurdu[a)]

AFFILIATIONS

Department of Materials Science and Nanotechnology Engineering, Abdullah Gül University, Kayseri 38080, Türkiye

Note: This paper is part of the special topic on Disordered Materials at the Atomic Scale.
[a)]**Author to whom correspondence should be addressed:** murat.durandurdu@agu.edu.tr

ABSTRACT

This study investigates the atomic structure, bonding, and electrical and mechanical properties of amorphous silicon boron nitride (a-Si_2BN) using *ab initio* molecular dynamics simulations. The simulations reveal a distinct phase-separated structure comprising Si-rich and BN-rich domains. BN layers are embedded within the amorphous Si matrix, with only a few bridging atoms linking these regions. The Si-rich region exhibits topological similarities to amorphous silicon, albeit with notable structural distortions. Electronic structure calculations indicate semiconducting behavior with a small bandgap, while mechanical property analysis shows a moderate bulk modulus and Young's modulus, achieving a balance between rigidity and elasticity. These findings position a-Si_2BN as a promising material for advanced applications, including flexible electronics, high-temperature semiconductors, and energy storage devices. While the proposed structure is currently hypothetical, its potential experimental realization could open new avenues in material design for emerging technologies.

I. INTRODUCTION

Silicon boron nitride (Si_2BN), a two-dimensional (2D) material with remarkable properties, has gained significant attention in recent years.[1–18] Its unique combination of mechanical strength, thermal stability, and electronic properties makes it a promising candidate for numerous applications, including energy storage, catalysis, and electronic devices.[3–18] The experimental realization of layered Si_2BN remains challenging, though its potential for environmental and energy-related applications is substantial.

In the broader context, 2D materials often exhibit properties distinct from their bulk counterparts. While much research on Si_2BN has focused on its 2D structures, interest in its bulk configurations has also grown. A recent theoretical study emphasized the potential of three-dimensional (3D) porous Si_2BN in various fields, particularly for energy storage.[19] Using the particle swarm optimization algorithm and first-principles calculations, researchers predicted the most likely structure for bulk Si_2BN, identified as α-Si_2BN with (P-4m2) symmetry.[20] This semiconducting material exhibits an extremely narrow indirect bandgap of 0.02 eV, combined with high hardness and a significant melting point, making it a promising candidate for high-temperature applications.

Amorphous forms of silicon boron nitride (a-SiBN) ceramics have also attracted considerable attention for their outstanding thermal and mechanical properties.[21–31] However, the amorphous form of Si_2BN (a-Si_2BN) remains largely unexplored. This study aims to fill this gap by investigating the atomic structure, electronic behavior, and mechanical properties of a- Si_2BN using *ab initio* molecular dynamics (MD) simulations.

The findings presented here contribute to a deeper understanding of a-Si_2BN and highlight its potential for various advanced applications. Specifically, the combination of thermal stability from the BN-rich domains, semiconducting behavior with a small bandgap, and mechanical flexibility suggests that a-Si_2BN could be a promising candidate for flexible electronics, high-temperature semiconductors, and energy storage devices. These applications benefit from the unique phase-separated structure and the balance between rigidity and elasticity observed in a-Si_2BN.

II. COMPUTATIONAL METHOD

The MD simulations were performed using the SIESTA *ab initio* program.[32] A pseudopotential approach[33] and the Perdew–Burke–Ernzerhof (PBE) generalized gradient approximation (GGA)

functional,[34] along with Grimme's dispersion correction,[35] were employed. The Brillouin zone was sampled at the Γ point, and double-zeta basis functions were used for the MD calculations. Self-consistency energy tolerance was set to 10^{-4} eV. A time step of 1.0 fs was applied for each MD step, and temperature control was achieved via velocity scaling within an isothermal-isobaric (NPT) ensemble. The Parrinello–Rahman method[36] was employed to maintain zero pressure during simulation.

To generate an a-Si_2BN structure, we employed the traditional melt-and-quench technique. The starting configuration was an amorphous B_4C model, modified by replacing some B and C atoms with Si and N atoms to achieve the desired Si_2BN composition (96 Si, 48 B, and 48 N atoms). This process is referred to as *Simulation 1*. The initial configuration was heated to 5000 K for 100 ps, followed by quenching to 300 K at a rate of 2×10^{13} K/s. The resulting structure at 300 K was then optimized using the conjugate gradient method, where both atomic positions and lattice parameters were relaxed until the maximum atomic force and stress were below 0.01 eV/Å and 0.02 GPa, respectively. The final amorphous structure had a density of 2.1997 g/cm^3.

To confirm that the starting structure has no significant effect on the final configuration, we performed an additional simulation, referred to as *Simulation 2*. In this case, the starting configuration was a C_2BN, which was modified by replacing all C atoms with Si to create an Si_2BN structure. The system was then thermalized at 2200 K for 50 ps. The resulting structure was compared to the results of Simulation 1 at the same temperature using partial pair distribution functions (PPD), as shown in Fig. 1. Notably, both simulations—despite differing in initial configurations and thermal conditions—produced similar structural motifs as exposed in Fig. 2, suggesting that the phase-separated Si_2BN structure represents the lowest-energy configuration.

Atomistic-level analysis and visualization of the structures were performed using the ISAACS[37] and VESTA[38] programs, respectively.

III. RESULTS

A. Structural properties

Figure 2 presents a ball-and-stick model of the computer-generated a-Si_2BN structure, highlighting its distinct phase-separated configuration. The model reveals Si-rich and BN-rich domains, with BN layers embedded within an amorphous Si (a-Si) matrix. These domains are interconnected by only a few bridging atoms. Similar BN layer formations have been reported in other a-SiBN structures[28,39] and B-doped Si_3N_4/SiC ceramics,[29] indicating that this feature is not unique to a-Si_2BN.

To examine the local atomic structure in detail, we first perform PPD analysis as exposed in Fig. 3. The results confirm the amorphous nature of the structure and show a complex network of bonds between various atomic species, notably without any N–N bonds. A prominent peak at 2.41 Å for Si–Si bonding is observed, falling between the bond lengths reported for a-$Si_3B_3N_7$ (2.56 Å)[31] and a-Si (2.35–2.38 Å).[40–43] This intermediate bond length suggests a unique bonding character in a-Si_2BN. The B–N bond length is approximately 1.44 Å, which aligns with both BN structures[44] and a-$Si_3B_3N_7$ (1.43–1.44 Å).[30,31] Additionally, a weak peak at 1.67 Å in the B–B correlation hints at the presence of a small number B–B bonds, with a bond distance smaller than the 1.70 Å observed in a-BC_5.[45] The B–Si bond is measured at 2.17 Å, shorter than the 2.72–2.75 Å in a-$Si_3B_3N_7$.[30,31] Finally, the Si–N bond distance is found to be 1.84 Å, longer than the 1.72–1.74 Å range reported for a-$Si_3B_3N_7$.[30,31] Overall, the PPD analysis reveals a complex and interconnected atomic structure in the a-Si_2BN system, with bond distances that deviate from those observed in other related materials as expected, due to the significant structural differences among them.

To further elucidate the local atomic environment within the simulated a-Si_2BN model, a coordination number analysis is conducted using predefined bond length thresholds (B–B = 1.89 Å, B–Si = 2.38 Å, Si–Si = 2.90 Å, B–N = 1.92 Å, and Si–N = 2.06 Å). The analysis reveals distinct trends in the coordination preferences of each element. Si atoms exhibit a mean coordination number of 3.95, with a strong preference for Si–Si bonds (3.66) and relatively few Si–N (0.16) and Si–B (0.12) bonds. N atoms demonstrate a mean coordination number of 3.02, primarily forming N–B bonds (2.68) with fewer N–Si bonds (0.33). B atoms have a mean coordination number of 3.06, with a significant preference for B–N bonds (2.68) and fewer B–Si (0.25) and B–B (0.12) bonds. Considering the overall structure of the model, these coordination numbers are comparable to those observed in a-Si with a mean coordination number of about 4.0 and a-BN with a mean coordination number of about 3.0.

The analysis of chemical environments, as summarized in Table I, highlights the most common bonding configurations in the

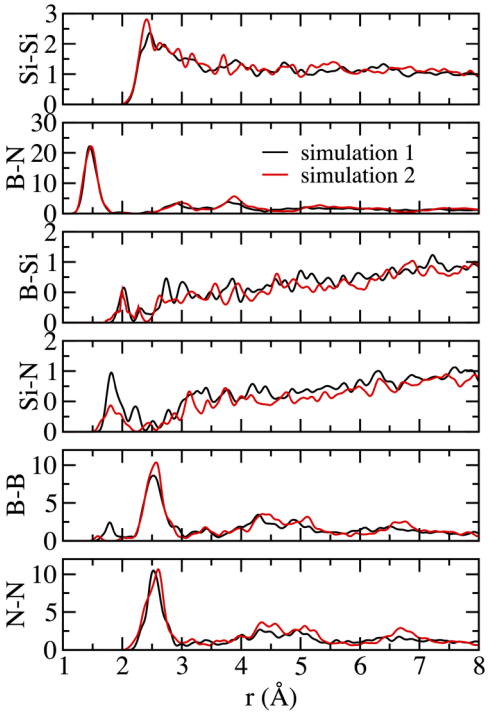

FIG. 1. PPD functions of the Si_2BN structures at 2200 K from two independent simulations with different starting configurations.

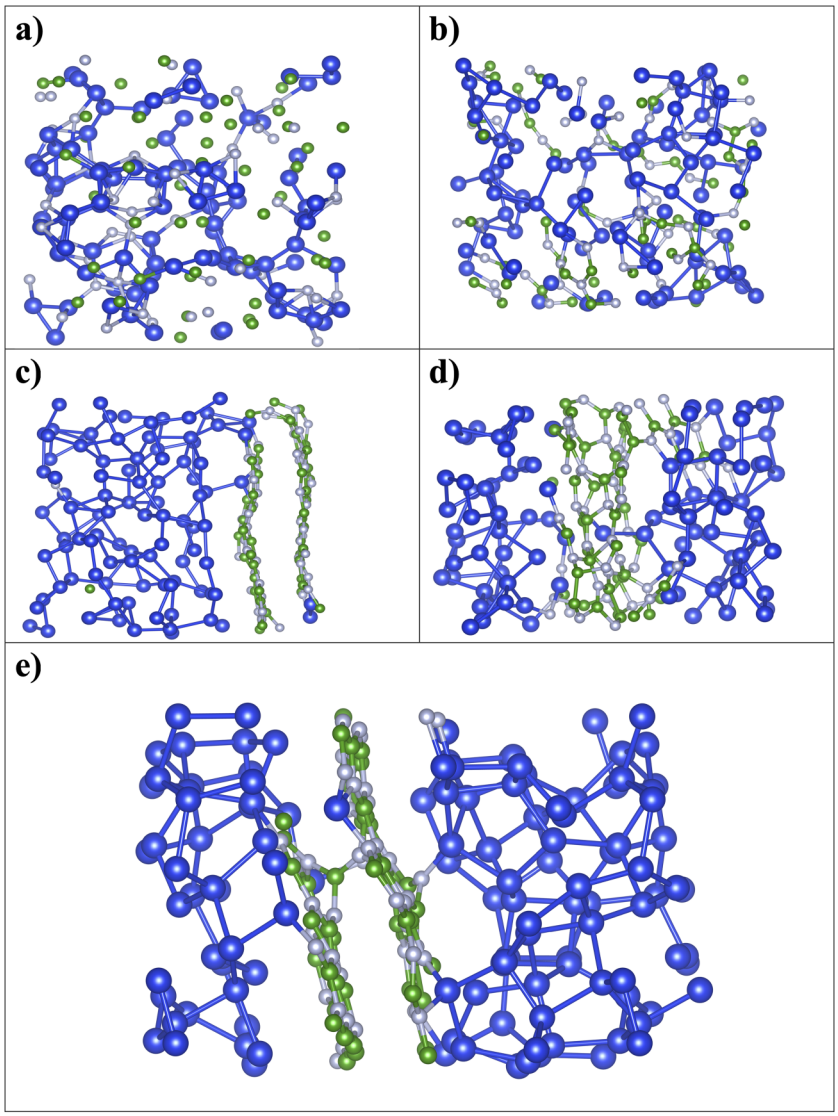

FIG. 2. Ball-and-stick representations of Si_2BN structures. (a) and (b) are the starting configurations. (c) and (d) are the structures at 2200 K. (e) is the fully relaxed structure after quenching to 300 K from *simulation 1*. Blue, green, and gray spheres represent Si, B, and N atoms, respectively.

a-Si_2BN structure. Approximately 91.7% of Si atoms are fourfold coordinated, with the majority (72.92%) existing in a $Si–Si_4$ configuration. A smaller fraction of Si atoms exhibit either threefold or fivefold coordination, indicating some variability in the local bonding environment. Most B atoms (93.7%) are threefold coordinated, predominantly forming a $B–N_3$ configuration (75.0%), while the remaining B atoms are fourfold coordinated. Similarly, the majority of N atoms (97.9%) are threefold coordinated, primarily in an $N–B_3$ arrangement (70.0%). The remaining N atoms display fourfold coordination.

To gain deeper insights into the atomic structure, we evaluate the bond angle distribution functions. Figure 4 presents the distributions for the most prevalent bonding configurations in the a-Si_2BN structure. The B–N–B and N–B–N bond angles exhibit a sharp peak around 120°, characteristic of a trigonal planar geometry typical of BN-rich domains, where B and N atoms adopt sp^2 hybridization. In contrast, the Si–Si–Si bond angle distribution is broader, with a peak centered around 105°. This significant deviation from the ideal tetrahedral angle of 109.5° reflects structural distortions in the Si-rich regions. These distortions likely contribute to the observed elongation of the mean Si–Si bond length compared to that in a-Si.

B. Electrical properties

The electron density of states (EDOS) consideration of the simulated a-Si_2BN model, as illustrated in Fig. 5, indicates a semimetallic character, as no clear forbidden gap is observed. Due to the Gaussian broadening of 0.15 eV applied in the plotting, the focus shifts to the energy difference between the highest occupied molecular orbital (HOMO) and the lowest unoccupied molecular orbital

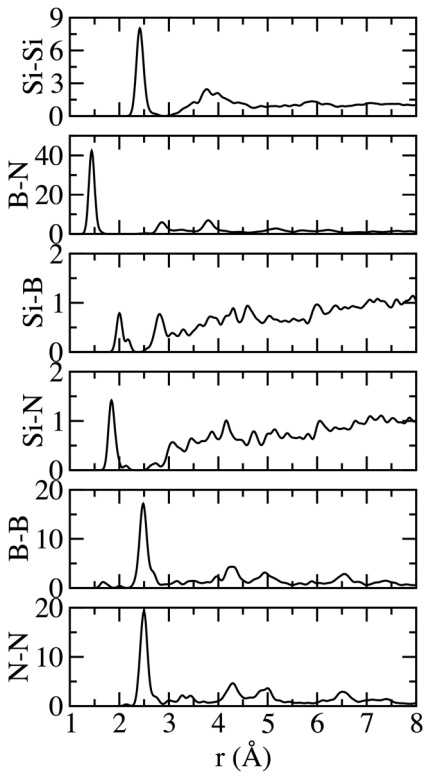

FIG. 3. PPD functions of the a-Si_2BN configuration.

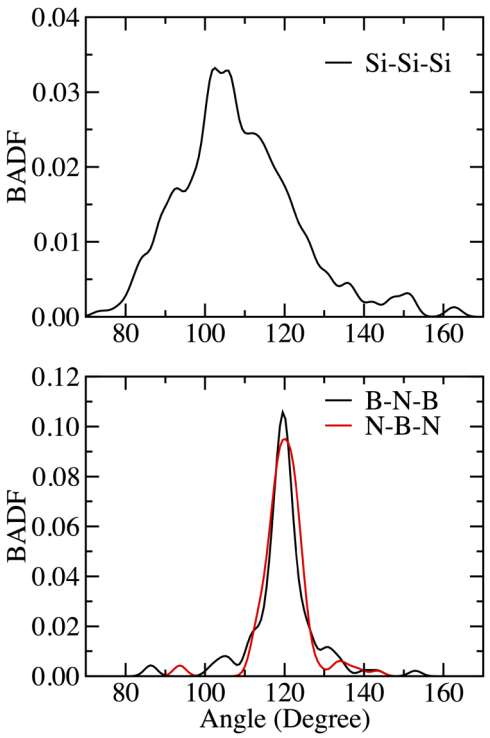

FIG. 4. Bond angle distribution functions (BADF) in a-Si_2BN.

(LUMO), which is estimated to be approximately 0.13 eV—larger than the 0.02 eV reported for α-Si_2BN.[20] The partial density of states (PDOS) analysis further elucidates the electronic structure. Si-p states dominate both the valence and conduction bands, indicating that Si atoms play a central role in determining the electronic behavior of the material. N-p states contribute primarily to the valence band, while B-p states are more prominent in the conduction band. This distribution suggests that the electronic structure is primarily governed by the Si atoms, with B and N acting as modifiers that refine the material's overall electronic properties.

It is important to note the inherent limitations of DFT-GGA, which is known to underestimate bandgaps. As such, the experimentally measured bandgap of a-Si_2BN is expected to exceed the predicted value of 0.13 eV, indicating the potential for semiconducting behavior under experimental conditions.

TABLE I. Identification of bonding around each species in the amorphous configuration.

Si		B		N	
Si_4	72.92%	N_3	75.00%	B_3	70.83%
Si_3B	7.29%	NSi_2	10.42%	B_2Si	22.92%
Si_3N	5.21%	N_2B	6.25%	BSi_2	4.17%
Si_3	5.21%	N_2SiB	4.17%	B_3Si	2.08%
Si_5	2.08%	NSiB	2.08%		
Si_2BN	2.08%	Si_4	2.08%		
SiN_3	1.04%				
Si_2N	1.04%				
Si_2B_2	1.04%				
Si_2N_2	1.04%				
N_3B	1.04%				

C. Mechanical properties

We estimate the bulk modulus (K) of a-Si_2BN by analyzing the energy (E) as a function of volume (V) using a variable cell optimization method. The energy–volume (E–V) relationship given in Fig. 6 is determined under hydrostatic conditions, with applied pressures ranging from −3 to 8 GPa. This simulation allows both atomic positions and cell parameters to adjust, accommodating changes in cell shape and atomic coordinates. The data are then fitted to the third-order Birch–Murnaghan equation of state,

$$E(V) = E_0 + \frac{9V_0K}{16}\left\{\left[\left(\frac{V_0}{V}\right)^{\frac{2}{3}} - 1\right]^3 K' + \left[\left(\frac{V_0}{V}\right)^{\frac{2}{3}} - 1\right]^2 \left[6 - 4\left(\frac{V_0}{V}\right)^{\frac{2}{3}}\right]\right\},$$

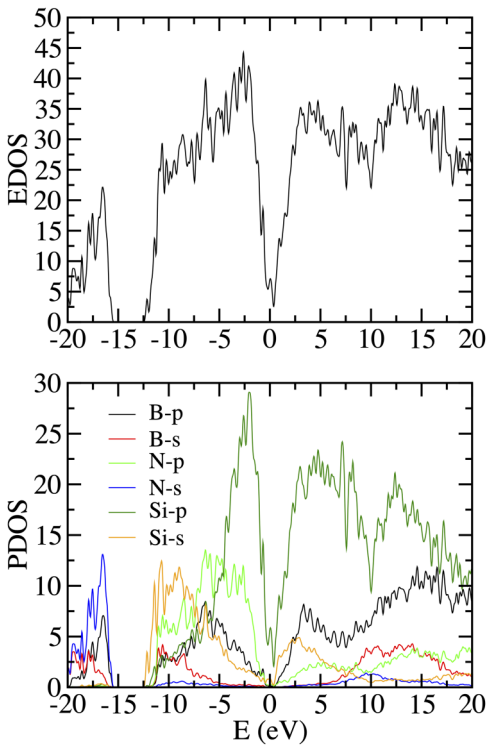

FIG. 5. Total and partial electron density of states of a-Si_2BN. The Fermi level is at 0 eV.

where V_0 is the equilibrium volume and K′ is its pressure derivative. This fitting allows us to accurately estimate the bulk modulus of a-Si_2BN based on the response of the material to volumetric changes under different pressure conditions. The calculated bulk modulus for a-Si_2BN is approximately 60 GPa, with K′ = 4.67. This value is intermediate between the bulk modulus of BN at 36.7 GPa[46] and that of a-Si at 106 GPa.[47] Depending on the specific density, the bulk modulus of related compositions, such as a-$Si_3B_3N_7$, could potentially fall within the 50–250 GPa range.[23] This intermediate value suggests that a-Si_2BN balances the flexibility of BN with the hardness of a-Si, making it an intriguing candidate for applications requiring moderate mechanical resilience.

To assess Poisson's ratio (ν) of a-Si_2BN, we apply uniaxial stress along the diagonal vector of the simulation cell, allowing the remaining stress components to relax to zero. During this process, both atomic positions and cell vectors are optimized. From the relationship between lateral strain ($\varepsilon_{lateral}$) and applied strain ($\varepsilon_{applied}$), as shown in Fig. 7, we derive Poisson's ratio using the following equation:

$$\nu = -\frac{\varepsilon_{lateral}}{\varepsilon_{applied}}.$$

Poisson's ratio exhibits significant directional dependence, with values ranging from 0.12 to 0.51. The lowest values

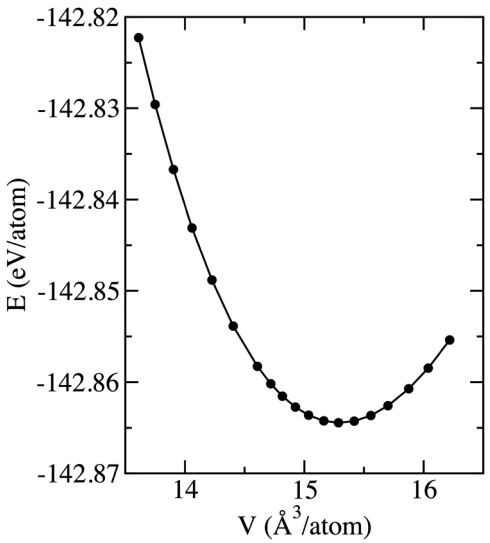

FIG. 6. Energy variation as a function of volume for the a-Si_2BN structure.

correspond to loading directions nearly perpendicular to the BN layer orientation, while the highest values occur when loading is more closely aligned with the BN layers. This pronounced anisotropy arises from the strong in-plane bonding within the BN layers. By averaging the six computed values, Poisson's ratio for a-Si_2BN is determined to be 0.23, closely aligning with the reported value of 0.27 for a-Si3B3N7 at 300 K.[48] This suggests that a-Si_2BN exhibits

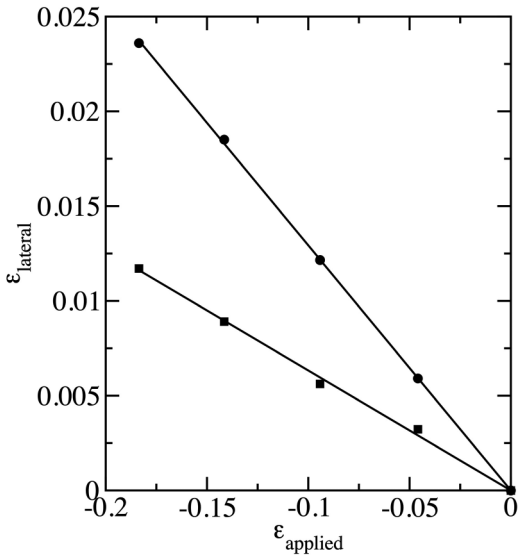

FIG. 7. The relationship between lateral strain ($\varepsilon_{lateral}$) and applied strain ($\varepsilon_{applied}$) for uniaxial stress along the x-direction in a-Si_2BN.

similar mechanical behavior, particularly in its resistance to deformation under applied stress.

Young's modulus (E) of a-Si2BN, representing its resistance to elastic deformation, is calculated as

$$E = 3K(1 - 2\upsilon).$$

The resulting Young's modulus is approximately 97 Gpa, lower than the reported 136 ± 9 GPa for a-Si,[49] 132 GPa for a-$Si_3B_3N_7$ at 300 K,[48] and ~200 GPa for a-SiBN ceramics.[28] This difference proposes that a-Si_2BN is comparatively less rigid and exhibits greater elasticity than both a-Si and a-SiBN, making it potentially more suitable for applications requiring flexibility in addition to mechanical strength.

The shear modulus (μ) is derived from Young's modulus and Poisson's ratio using the following formula:

$$\mu = \frac{E}{2(1+\nu)}.$$

For a-Si_2BN, the shear modulus is estimated to be around 40 GPa, which is higher than the 33 GPa reported for a-Si,[47] reflecting a-Si_2BN's greater capacity to withstand shear forces, highlighting its improved mechanical performance in applications that involve torsional or shear stress.

In order to compute the Vickers hardness (H) of a-Si_2BN, we employ four empirical relationships that are widely cited in the literature for hardness prediction.[50–53] The following equations are used:

$$H = 0.151\mu,$$

$$H = 0.92\left(\frac{1}{n}\right)^{1.137}(\mu)^{0.708},$$

$$H_v = 2\left(\frac{\mu}{n^2}\right)^{0.585} - 3 \text{ (GPa)},$$

$$H = 0.0635E.$$

In these equations, n represents Pugh's ratio (K/μ). The estimated hardness for a-Si_2BN falls between 5.9 and 7.7 GPa depending on the equation used, which is lower than the reported hardness of 10.9 ± 0.9 GPa for a-Si.[49] These values indicate that while a-Si_2BN possesses moderate hardness, it is not as hard as a-Si or conventional Si-based ceramics, making it more suited for applications where a balance between hardness and flexibility is required.

IV. DISCUSSION

This study offers valuable insights into the structural, electronic, and mechanical properties of a-Si_2BN, highlighting its potential for various technological applications. One of the key findings is the unique phase-separated structure of a-Si_2BN, which features distinct Si-rich and BN-rich domains. The embedded BN layers within the amorphous Si matrix, along with the structural distortions observed in the Si-rich regions, contribute to the material's distinct characteristics. These distortions may impact both the mechanical flexibility and the electronic properties by influencing the density of states near the Fermi level, potentially reducing stiffness while modifying charge transport.

From a mechanical perspective, the calculated properties—such as a bulk modulus of 60 GPa, Young's modulus of 97 GPa, and a Vickers hardness ranging from 5.9 to 7.7 GPa—indicate that a-Si_2BN is relatively hard but less rigid than other ceramics like a-$Si_3B_3N_7$. The BN-rich domains, known for their layered structures, likely contribute to the material's flexibility, while the Si-rich regions enhance hardness. This combination could be advantageous in applications where both durability and flexibility are required. The moderate Poisson's ratio (0.23) and bulk modulus suggest good resistance to mechanical deformation and thermal expansion. Additionally, the BN-rich regions may improve the material's thermal conductivity and stability, making a-Si_2BN a strong candidate for high-temperature electronic applications.

On the electronic side, a-Si_2BN exhibits semiconducting behavior with a small bandgap of 0.13 eV. Although this gap is smaller than expected—due to the limitations of DFT-GGA in underestimating bandgaps—more accurate predictions can be achieved using advanced techniques like hybrid functionals or GW calculations. The bandgap tunability through compositional or structural modifications offers potential for a-Si_2BN in optoelectronic applications and thermoelectric devices, where control over electronic properties is crucial. Overall, the combination of flexibility, mechanical strength, and moderate electronic conductivity opens up exciting possibilities for a-Si_2BN in various fields, ranging from high-temperature electronics to flexible optoelectronics.

While the size of the amorphous model used in this study is considerable for *ab initio* simulations, potential size effects cannot be entirely discounted. The smaller model size may limit the ability to capture the full spectrum of structural and compositional variations in a-Si_2BN, which could affect the generalizability of the results. For example, in larger systems, distortions in the Si-rich domains might be less pronounced, and the distribution of BN layers may show greater nonuniformity. Although these factors are unlikely to significantly influence short-range order, they may impact microscopic properties, such as mechanical moduli and electronic behavior. To achieve a more comprehensive understanding of the local structure and properties of a-Si_2BN, future studies should focus on simulations with larger models or ensembles of configurations. Such efforts would refine the observed trends and further validate the conclusions drawn from this work.

V. CONCLUSIONS

In conclusion, this study provides a comprehensive investigation into the atomic structure, bonding, and electronic properties of a-Si_2BN. The unique phase-separated structure, coupled with its semiconducting nature and favorable mechanical properties, positions a-Si_2BN as a promising material for a range of applications, including flexible electronics, energy storage devices, and beyond. The balance between hardness and flexibility, along with its electronic properties, suggests that a-Si_2BN holds significant potential in emerging technologies. To validate these theoretical predictions,

experimental synthesis and mechanical testing of a-Si_2BN are essential steps for further exploration of its practical applications.

ACKNOWLEDGMENTS

The author extends gratitude to the Abdullah Gül University Support Foundation for their support. The author acknowledges the computing resources and time generously provided by TÜBİTAK ULAKBİM High Performance and Grid Computing Center (TRUBA resources).

AUTHOR DECLARATIONS

Conflict of Interest

The author has no conflicts to disclose. During the preparation of this work, the author used some AI tools in order to improve the language. After using this tool/service, the author reviewed and edited the content as needed and takes full responsibility for the content of the publication.

Author Contributions

Murat Durandurdu: Conceptualization (equal); Data curation (equal); Formal analysis (equal); Funding acquisition (equal); Investigation (equal); Methodology (equal); Validation (equal); Visualization (equal); Writing – original draft (equal); Writing – review & editing (equal).

DATA AVAILABILITY

The data that support the findings of this study are available from the corresponding author upon reasonable request.

REFERENCES

[1]A. N. Andriotis, E. Richter, and M. Menon, Phys. Rev. B **93**, 081413 (2016).
[2]E. D. Sandoval, S. Hajinazar, and A. N. Kolmogorov, Phys. Rev. B **94**, 094105 (2016).
[3]H. R. Mahida, D. Singh, Y. Sonvane, S. K. Gupta, P. B. Thakor, and R. Ahuja, New J. Chem. **45**, 3892 (2021).
[4]H. Abdelsalam, M. Ali, N. H. Teleb, M. M. Ibrahim, M. A. Ibrahim, and Q. Zhang, Chem. Phys. Lett. **772**, 138568 (2021).
[5]D. Singh, S. K. Gupta, Y. Sonvane, T. Hussain, and R. Ahuja, Phys. Chem. Chem. Phys. **20**, 21716 (2018).
[6]S. Hu, Y. Yong, C. Li, Z. Zhao, H. Jia, and Y. Kuang, Phys. Chem. Chem. Phys. **22**, 13563 (2020).
[7]H. Abdelsalam, M. Ali, N. H. Teleb, M. M. Ibrahim, M. A. Ibrahim, and Q. Zhang, Chem. Phys. Lett. **772**, 138568 (2021).
[8]M. Jiang, J. Xu, P. Munroe, Z. H. Xie, and Z. Chen, Int. J. Hydrogen Energy **50**, 865 (2024).
[9]D. Singh, S. Chakraborty, and R. Ahuja, ACS Appl. Energy Mater. **2**, 8441 (2019).
[10]P. Panigrahi, S. B. Mishra, T. Hussain, B. R. K. Nanda, and R. Ahuja, ACS Appl. Nano Mater. **3**, 9055 (2020).
[11]P. Panigrahi, Y. Pal, R. Ahuja, and T. Hussain, Energy Fuel **35**, 12688 (2021).
[12]D. Singh, S. K. Gupta, Y. Sonvane, and R. Ahuja, Int. J. Hydrog. Energy **42**, 22942 (2017).
[13]H. R. Mahida, D. Singh, Y. Sonvane, P. B. Thakor, R. Ahuja, and S. K. Gupta, J. Appl. Phys. **126**, 23 (2019).
[14]S.-J. Yuan, H. Zhang, and X.-L. Cheng, Plasmonics **13**, 947 (2018).
[15]D. Singh, P. K. Panda, N. Khossossi, Y. K. Mishra, A. Ainane, and R. Ahuja, Catal. Sci. Technol. **10**, 3279 (2020).
[16]T. Hussain, D. Singh, S. K. Gupta, A. Karton, Y. Sonvane, and R. Ahuja, Appl. Surf. Sci. **469**, 775 (2019).
[17]V. Shukla, J. Wärnå, N. K. Jena, A. Grigoriev, and R. Ahuja, J. Phys. Chem. C **121**, 26869 (2017).
[18]V. Shukla, R. B. Araujo, N. K. Jena, and R. Ahuja, Nano Energy **41**, 251 (2017).
[19]U. Younis, I. Muhammad, W. Wu, S. Ahmed, Q. Sun, and P. Jena, Nanoscale **12**, 19367 (2020).
[20]J. Wang, S. Chen, Y. Yang, Y. Yu, H. Dong, and Y. Li, Diamond Relat. Mater. **130**, 109530 (2022).
[21]R. M. Hagenmayer, U. Müller, C. J. Benmore, J. Neuefeind, M. Jansen, J. Mater. Chem. **9**, 2865 (1999).
[22]A. Dasmahapatra and P. Kroll, J. Am. Ceram. Soc. **101**, 3489 (2018).
[23]J. C. Schön, A. Hannemann, G. Sethi, V. Pentin, M. Jansen, Process. Appl. Ceram. **5**, 49 (2011).
[24]U. Müller, W. Hoffbauer, and M. Jansen, Chem. Mater. **12**, 2341 (2000).
[25]G. Jeschke, M. Kroschel, and M. Jansen, J. Non-Cryst. Solids **260**, 216 (1999).
[26]D. Heinemann, W. Assenmacher, W. Mader, M. Kroschel, and M. Jansen, J. Mater. Res. **14**, 3746 (1999).
[27]X. Long, C. Shao, and Y. Wang, J. Am. Ceram. Soc. **103**, 4436 (2020).
[28]J. Al-Ghalith, A. Dasmahapatra, P. Kroll, E. Meletis, and T. Dumitrică, J. Phys. Chem. C **120**, 24346 (2016).
[29]Y. Zhan, W. Li, T. Jiang, C. Fasel, E. Ricohermoso, J. Bernauer, Z. Yu, Z. Wu, F. Müller-Plathe, L. Molina-Luna, R. Grottenmüller, and R. Riedel, J. Adv. Ceram. **11**, 1104 (2022).
[30]A. Hannemann, J. C. Schön, M. Jansen, H. Putz, T. Lengauer, Phys. Rev. B **70**, 144201 (2004).
[31]T. T. Nguyen, T. C. Dinh, T. T. Nguyen, and V. V. Le, J. Non-Cryst. Solids **615**, 122431 (2023).
[32]J. M. Soler, E. Artacho, J. D. Gale, A. García, J. Junquera, P. Ordejón, D. Sánchez-Portal, J. Phys.: Condens. Matter **14**, 2745 (2002).
[33]N. Troullier and J. L. Martins, Phys. Rev. B **43**, 1993 (1991).
[34]J. P. Perdew, K. Burke, and M. Ernzerhof, Phys. Rev. Lett. **77**, 3865 (1996).
[35]S. Grimme, J. Comput. Chem. **27**, 1787 (2006).
[36]M. Parrinello and A. Rahman, J. Appl. Phys. **52**, 7182 (1981).
[37]S. Le Roux and V. Petkov, J. Appl. Crystallogr. **43**, 181 (2010).
[38]K. Momma and F. Izumi, J. Appl. Crystallogr. **44**, 1272 (2011).
[39]N. Liao, W. Xue, H. Zhou, M. Zhang, Int. J. Mater. Res. **104**, 162 (2013).
[40]R. Bellissent, A. Chenevas-Paule, P. Chieux, A. Menelle, J. Non-Cryst. Solids **77**, 213 (1985).
[41]J. F. Graczyk and D. J. J. D. Fischer, Phys. Status Solidi A **55**, 231 (1979).
[42]A. Filipponi, M. S. L. M. A. P. Roy, and S. E. C. Fridkin, J. Phys. Colloq. **47**, 375 (1986).
[43]D. Igram, B. Bhattarai, P. Biswas, and D. A. Drabold, J. Non-Cryst. Solids **492**, 27 (2018).
[44]Y. Kumashiro, *Electric Refractory Materials* (Taylor & Francis, New York, 2000).
[45]M. Durandurdu, J. Non-Cryst. Solids **592**, 121743 (2022).
[46]V. L. Solozhenko, G. Will, and F. Elf, Solid State Commun. **96**, 1 (1995).
[47]M. D. Kluge and J. R. Ray, Phys. Rev. B **37**, 4132 (1988).
[48]M. Griebel and J. Hamaekers, Comput. Mater. Sci. **39**, 502 (2007).
[49]D. M. Follstaedt, J. A. Knapp, and S. M. Myers, J. Mater. Res. **19**, 338 (2004).
[50]D. M. Teter, MRS Bull. **23**, 22 (1998).
[51]X. Q. Chen, H. Niu, D. Li, and Y. Li, Intermetallics **19**, 1275 (2011).
[52]Y. Tian, B. Xu, and Z. Zhao, Int. J. Refract. Met. Hard Mater. **33**, 93 (2012).
[53]X. Jiang, J. Zhao, A. Wu, Y. Bai, and X. Jiang, J. Phys.: Condens. Matter **22**, 315503 (2010).